ChemComm

Accepted Manuscript

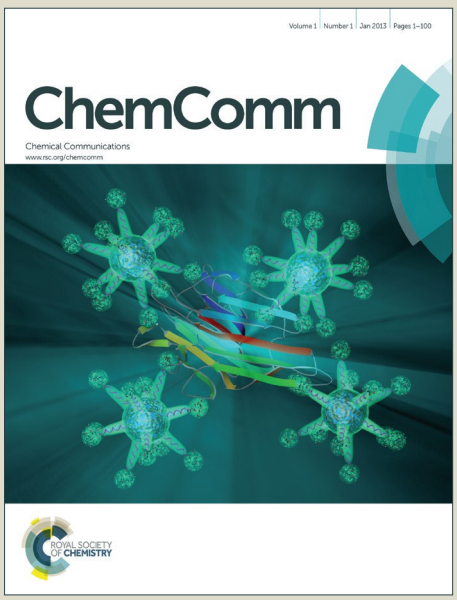

ROYAL SOCIETY OF CHEMISTRY

www.rsc.org/chemcomm

Journal Name

COMMUNICATION

Graphene Modified Mesoporous Titania Single Crystals with Controlled and Selective Photoredox Surfaces

Received 00th January 20xx,
Accepted 00th January 20xx

DOI: 10.1039/x0xx00000x

www.rsc.org/

Yi Zhou,[a] Qiuying Yi,[a] Mingyang Xing,*[a] Lu Shang,[b] Tierui Zhang,*[b] and Jinlong Zhang*[a]

A sandwich structured graphene modified TiO_2 mesoporous single crystals (GR-MSCs) by using the graphene embedded silica spheres as the hard template, via a hydrothermal treatment. The selective photocatalysis of TiO_2 can be achieved by controlling the location of graphene in TiO_2 mesoporous single crystals. The sandwich structured graphene-TiO_2 composite has a photooxidation surface, and the core-shell structured TiO_2@graphene has a photoreduction surface. It provides a new pathway to realize the selectivity of photocatalysis by controlling the location of graphene in the TiO_2 MSCs for the first time.

Recently, mesoporous TiO_2 single crystals (MSCs) have attracted much attention for their large specific surface areas, perfect single-crystalline structures, catalytically active facets, and capacities for high electron mobility.[1-3] However, MSCs do not afford the low recombination rates of electrons and holes necessary for effective photo-catalysis. This is especially true for micrometer scale MSCs that produce extremely high recombination rates in the bulk or on the TiO_2 surface, resulting in low photo-catalytic activities.[4] The use of graphene may address this limitation, because graphene is an ideal electron attractor and can be expected to facilitate the separation of electrons and holes.[5] However, most research on TiO_2/graphene composites has been focused on loading TiO_2 nanoparticles onto graphene surfaces or wrapping the surfaces of TiO_2 spheres with graphene.[6-18] Remarkably, inserting graphene into the bulk of pure TiO_2 single crystals can result in micrometer-scale crystals with effective electron attractors. Combined with the exposure of high energy facets, this technique can be used to enhance the separation of electrons and holes, potentially resolving the low photo-oxidation efficiency inherent to conventional TiO_2 single crystals. Until now, to the best of our knowledge, graphene sheets have not been successfully inserted into the bulk of TiO_2 single crystals. This challenge likely stems from the difficulties associated with preparing graphene modified TiO_2 sandwiched composites that results from the closely packed growth pattern of solid single crystals of TiO_2.

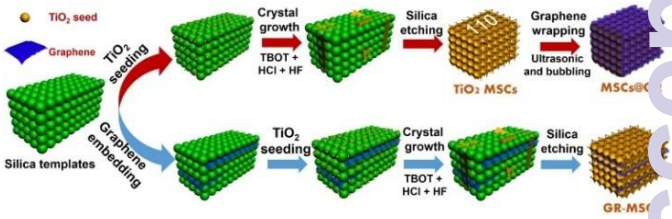

Fig. 1 Schematic illustration of the growth pathways of core-shell structured MSCs@GR and sandwich structured GR-MSCs.

Here, we report the first successful preparation of sandwiched graphene-modified TiO_2 MSC composites (GR-MSCs). These materials were prepared by a hydrothermal method with graphene-embedded silica spheres as the hard template. The sandwiched graphene of the GR-MSCs serves as an electron attractor and site for electron accumulation. As a result, the holes prefer to transfer to the surface of the exposed (110) facet due to the high surface energy found there.[19-22] This directional electron transfer significantly reduces the recombination of electrons and holes in these composites. Through this mechanism, GR-MSCs exhibit highly active surfaces for photo-oxidation. To highlight the unique and useful properties of sandwiched GR-MSCs, control materials comprised of core-shell structured TiO_2/graphene composites (mesoporous composites of MSCs@GR and solid composites of TiO_2@graphene) were also prepared by an ultrasonic-bubbling method that affords selective photo-reduction surfaces. By controlling the location of graphene in the TiO_2 MSCs with exposed (110) facets, rapid and selective photo-catalysis can be achieved.

[a] Key Laboratory for Advanced Materials and Institute of Fine Chemicals, East China University of Science and Technology, 130 Meilong Road, Shanghai 200237, P.R. China E-mail: mingyangxing@ecust.edu.cn; jlzhang@ecust.edu.cn.
[b] Key Laboratory of Photochemical Conversion and Optoelectronic Materials Technical Institute of Physics and Chemistry, Chinese Academy of Sciences, Beijing 100190, P.R. China. E-mail: tierui@mail.ipc.ac.cn

†Electronic Supplementary Information (ESI) available: Experimental details and additional figures are provided including Raman, XRD, UV–vis, TG, Nitrogen adsorption-desorption isotherms, TEM and elements mapping, XPS, FTIR, PL, Photocurrent responses, Adsorption capacity, Cycling tests. See DOI: 10.1039/x0xx00000x

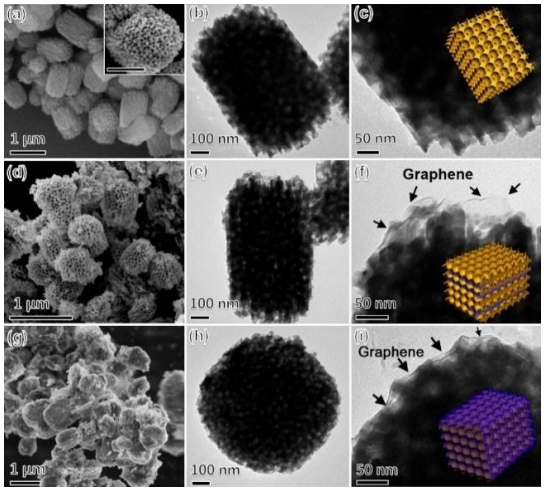

Fig. 2 SEM and TEM images for (a-c) TiO_2 MSCs (inset of (a) is the amplification of MSCs. Scale bar, 500 nm), (d-f) GR-MSCs and (g-i) MSCs@GR. Insets of (c), (f), (i) are the corresponding structure models.

Fig. 1 illustrates the process of inserting graphene into the TiO_2 MSCs by hydrothermal treatment. During the preparation of the silica template, the graphene oxides (GO) are dispersed into the spaces separating the closely packed silica spheres. The addition of seeds of TiO_2 crystals into the graphene-embedded silica template is vital for obtaining sandwiched GR-MSCs. The in situ growth of crystal seeds on the graphene surface induces the involvement of the graphene in the microcrystal lattice growth during the subsequent hydrothermal treatment. From this process, the graphene is introduced into the bulk of TiO_2. The graphene can also be wrapped around the surface of TiO_2 MSCs or solid single crystals to obtain core-shell structured MSCs@GR or TiO_2@graphene using a simple ultrasonic-bubbling method.

Raman and XRD spectra indicate that all the graphene-modified TiO_2 MSCs are of the same crystalline form as rutile and the successful reduction of GO in GR-MSCs and MSCs@GR (Fig. S1a,b). The concentration of graphene present in the composites can be quantified by thermo-gravimetric and differential thermal analyses (Fig. S2), which indicates the proportions of graphene in GR-MSCs and MSCs@GR are 8.94 % and 7.46 %, respectively. Interestingly, although the sandwiched GR-MSCs have a slightly higher concentration of graphene and absorb slightly more strongly compared to core-shell structured MSCs@GR (Fig. S3), the bandgap of GR-MSCs is almost identical to that of MSCs@GR (inset of Fig. S3). After modification with graphene, all the TiO_2 MSCs clearly feature enhanced absorptions in the visible light region. The absorption bands of GR-MSCs and MSCs@GR exhibit a significant redshift compared with the pure TiO_2 MSCs, owing to the generation of chemical bonds between TiO_2 and graphene.

The SEM and TEM images for different graphene-modified TiO_2 MSCs are shown in Fig. 2. The pure TiO_2 MSCs have the appearance of a perfect cuboid single crystal with exposed (110) facets and an ordered mesoporous structure (Fig. 2a). The pore size of this material is ~40 nm (inset of Fig. 2a). Also visible are channels of ~10-20 nm in diameter forming a 3D-network throughout the framework (Fig. 2b). The magnified images of the TiO_2 MSCs indicate that the edges of the MSCs are relatively smooth (Fig. 2c). The specific surface area of the MSCs is calculated to be 27.79 m^2/g. The type IV N_2 sorption isotherm curves and the Barrett-Joyner-Halenda pore size distribution centered at 40-50 nm also confirm the mesoporous nature of the structures (Fig. S4a,b). After the introduction of graphene into the TiO_2 MSCs, the MSCs decrease in size from 500-700 to 400-600 nm. This observation likely results from the inhibition of TiO_2 single crystal growth due to the introduction of graphene into the lattice (Fig. 2d). The absence of large, layered graphene suggests that most of the graphene has been incorporated into the MSCs. Compared with the smooth appearance of the surface of pure TiO_2 MSCs, the edges of GR-MSCs appear slightly rough because some fringe of sandwiched graphene are exposed to the surface (Fig. 2e,f). Interestingly, after the graphene is introduced into the bulk of the MSC, micropores of ~2 nm appear in the pore size distribution spectra shown in Fig. S4d. These features are indicative of aggregated pores resulting from the chemical linking between graphene and TiO_2. The presence of these micropores indicates that tight junctions between TiO_2 and graphene are present in the bulk of the MSCs instead of on the surface. Despite the strong chemical interaction between graphene and TiO_2 resulting from graphene's flexible nature, micropores were not produced by surface wrapping after graphene was chemically bonded to the surface of MSC (MSCs@GR) (Fig. S4e,f). In contrast to the GR-MSCs, the core-shell structured MSCs@GR feature a thin layer of graphene coated onto the surface of the MSCs (Fig. 2g-i). A uniform distribution of TiO_2 micro-single crystal aggregates in the graphene sheets, which has an appearance resembling beetles caught in a cobweb, is visible. MSCs@GR composites exhibit both crinkled and smooth textures that result from the presence of flexible and ultrathin graphene sheets (inset of Fig. 2i). TEM images confirm that the TiO_2 MSCs are firmly encapsulated by graphene sheets even after the composites were ultrasonically dispersed in order to enable TEM characterization. These features are indicative of strong interactions between MSC and graphene.TEM images of GR-MSC and MSCs@GR with different amount of graphene furtherly comfirms the sandwich and core-shell structure respectively.(Fig. S5) We choose a GR-MSC particle at random from the TEM image to record the SAED and characterize the lattice fringe (Fig. S6). The SAED pattern further confirms the single-crystal-like nature of the material (inset of Fig. S6a), and indicates that the exposed (110) facets are dominant in the TiO_2 MSCs (Fig. S6b).[23-25] The clear lattice fringes visible in Fig. S6c, d can be assigned with confidence to the (200) and (1$\bar{1}$0) spacings of rutile and are in good agreement with the SAED pattern. In order to further demonstrate the synthesized MSCs is indeed the mesoporous single crystal, the TEM image with proper magnificence was given in Fig. S6e, f to reveal the interface information on MSCs.

The element mapping images of TiO_2 MSCs and GR-MSCs presented in Fig. S7 and Fig. S8 confirm the presence of sandwich structured GR-MSCs. When graphene has been introduced into the bulk of the TiO_2 MSCs, many clearly

distinguishable red dots appear in the region corresponding to the bulk of the MSCs. And the absence of carbon at the edges of the GR-MSCs indicates that the graphene is indeed embedded inside the MSC, affording a sandwich-like structure (detailed discussion in the ESI).

The XPS spectra in Fig. S9 shed light on the catalytic effect of graphene in the systems investigated here. Compared to the reaction using blank TiO_2 MSCs, the use of sandwiched GR-MSCs affords a new peak at 288.3 eV resulting from the generation of Ti-O-C bonds between graphene and MSCs.[26, 27] When the graphene is wrapped around the surface of TiO_2 using an ultrasonic-bubbling treatment, the expected Ti-C bonds between TiO_2 and graphene are observed as indicated by the peaks appearing at 280.5 eV.[28-30] The FTIR results further confirm the interaction of TiO_2 with graphene (Fig. S10). The small peaks at 796 cm^{-1} and 1099 cm^{-1} are assigned to Ti-O-C bonds and Ti-C bonds, respectively.[6, 31]

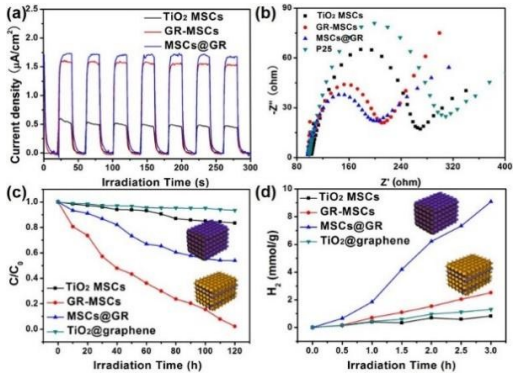

Fig. 3 (a) Transient photocurrent responses of different samples (300 W Xe lamp). (b) EIS changes of different samples in dark (The EIS measurements were performed in the presence of a 2.0 mM $K_3[Fe(CN)_6]$ and 0.5 M KCl mixture aqueous solution.). (c) Photo-oxidation activities for phenol degradation induced by simulated solar light (with an AM 1.5 air mass filter). (d) Solar light driven (with an AM 1.5 air mass filter) photo-catalytic water reduction for H2 generation.

The structural analysis of the graphene modified TiO_2 MSCs (either GR-MSCs or MSCs@GR) indicate that graphene has been introduced into the systems, potentially resulting in highly efficient electron transfer. Each of the graphene modified TiO_2 MSCs exhibit decreased solid-state photoluminescence (PL) signals compared with blank TiO_2 MSCs (Fig. S11). This effect suggests that the electron-hole recombination rate has been reduced by the addition of graphene.[32] Either coated on the surface or introduced into the bulk of TiO_2, graphene appears to be beneficial for the directional transfer of electrons. The fact that the specific surface areas of these materials are similar (32.05 m^2/g *vs.* 37.98 m^2/g) allows for the elimination of the possible effect of particle size on the electrochemical properties. Additionally, the photocurrent density of the GR-MSCs is similar to that of MSCs@GR and much higher compared to that of TiO_2 MSCs (1.60 $\mu A/cm^2$*vs.* 1.73 $\mu A/cm^2$*vs.* 0.53 $\mu A/cm^2$, Fig. 3a). The photocurrent density of GR-MSCs remains constant even after 1000 s of continuous illumination (Fig. S12), suggesting that sandwiched structure itself is highly stable. The impedance of GR-MSCs is also very close to that of MSCs@GR and much lower compared to that of blank TiO_2 MSCs and P25 (Fig. 3b). EIS changes of different samples under irradiation are similar to that in dark (Fig. S13). The impedance of blank TiO_2 MSCs is lower than that of commercial P25 owing to the presence of exposed (110) facets.[19]

Although the GR-MSCs and MSCs@GR have a similar electron-transfer efficiency and electron-hole separation, they have totally different photo-catalytic activities. For instance, the sandwiched GR-MSCs catalyze the rapid photo-oxidation of phenol but only mildly catalyze the photo-reduction of water to H_2 (Fig. 3c,d). The rate of light-dependent phenol oxidation for the sandwiched GR-MSCs is ~2.1 times greater than that of the core-shell structured MSCs@GR and ~15.0 times greater than that of the solid TiO_2@graphene composite (It shares a similar core-shell structure with the MSCs@GR, as shown in Fig. S14). Each catalyst tested here exhibits similarly low amounts of phenol adsorption in the dark (Fig. S15), but the GR-MSCs exhibits the greatest overall solar light-dependent photodegradation activity. With increasing amount of graphene, the photocayalytic activity of sandwich or core-shell structured graphene modified mesoporous TiO_2 single crystals was increased then decreased. The original GR-MSCs and MSC@GR present the highest photocatalytic activities respectively (Fig. S16). Moreover, GR-MSCs also shows the best photo-oxidation activity in the presence of Pt. (Fig. S17a) The unique sandwiched GR-MSCs maintain high photooxidation activities for the degradation of phenol even after 4 catalytic cycles, indicating high catalytic stability (Fig. S18). Conversely, the MSCs@GR catalyze the rapid photo-reduction of water for H_2 generation but only mildly catalyze the photo-oxidation of phenol (Fig. 3c, d). Moreover, the MSCs@GR with 0.377 wt% Pt loading shows the higher formation rate in the photocatalytic hydrogen generation and the photocatalyst without Pt loading shows no photocatalytic activity. (Fig. S17b) The rate of water photo-reduction for the MSCs@GR is ~3.6 times greater than that of the GR-MSCs and ~7.0 times greater than that of the solid TiO_2@graphene composite. These results indicate that selective photo-catalysis can be achieved by controlling the location of graphene in TiO_2.

Terephthalic acid was used as the probe to measure the ·OH concentration during the photocatalytic reaction. This was achieved by measuring the PL signal of ortho-hydroxyterephthalic acid (Fig. S19a).[32, 33] The concentration of ·OH indirectly reflects the concentration of photo-generated holes. Among the catalysts, GR-MSCs exhibited the strongest PL signal, indicating the greatest production of ·OH during the photocatalytic process. Upon the addition of hole trapping agents such as $Na_2S_2O_3$ to the solution containing the GR-MSCs, the resulting PL signal was greatly diminished. These results indicate that the GR-MSCs can produce many more holes on the MSC surface and are capable of photo-oxidative catalysis mainly under the solar light irradiation. Due to the lower potential of graphene, the photo-generated electrons prefer to transfer to the sandwiched graphene in the bulk of TiO_2 (Fig. S19c)[7, 13, 34, 35]. Simultaneously, the photo-generated holes tend to move to the exposed (110) facet due to the high

surface energy found there. Because phenol molecules are preferentially adsorbed to the surface of photocatalysts, the nature of this catalytic surface with regards to holes is vital to the catalytic photooxidation of this compound.

We employed Fe^{3+} as a probe to indirectly detect the electron concentration of different samples under solar light irradiation. Fe^{3+} is easily reduced to Fe^{2+} by photo-generated electrons. Fe^{2+} ions subsequently react with 1,10-phenanthroline monohydrate (Phen) to generate an orange product that absorbs strongly in the visual spectrum.[33] Measuring the concentration of this colored product indirectly gives the electron concentration. MSCs@GR affords the strongest absorption signal of all the catalysts tested, indicating that it produces the greatest Fe^{2+} concentration (Fig. S19b). Upon the addition of the electron trapping agent, $K_2S_2O_4$, to the solution containing MSCs@GR, the absorption signal disappears entirely, indicating that MSCs@GR have the highest electron concentration. The graphene coated onto the surface of MSCs enhances the aggregation of electrons onto the shell of the MSCs@GR. Although the holes prefer to move to the surface of the TiO_2 due to the exposed (110) facets, the graphene wrapped onto the MSC surface biases the directional electron transfer onto itself and inhibits the surface recombination of electrons and holes (Fig. S19c).

In summary, we have prepared the first sandwiched graphene-modified TiO_2 MSC composites using SiO_2 as a hard template. These materials exhibit excellent photo-oxidation properties compared with the conventional core-shell structured TiO_2@graphene composites. Unexpectedly, the location of the graphene in these materials appears to reliably dictate the selectivity of the catalysis. While conventional MSCs@GR are limited to featuring only a photoreduction surface, the sandwiched GR-MSCs described here also exhibited a unique photo-oxidation surface with catalytic activities greatly in excess of other core-shelled TiO_2@graphene composites. This work provides a new method to achieve selective photo-catalysis using TiO_2 and has potential applications in photo-catalytic organics synthesis and other selective redox reactions.

This work has been supported by National Nature Science Foundation of China (21203062, 21377038, 21173077, 21237003, 51322213, 21577036), the National Basic Research Program of China (973 Program, 2013CB632403), the Research Fund for the Doctoral Program of Higher Education (20120074130001), the Fundamental Research Funds for the Central Universities (22A201514021), and sponsored by "Chenguang Program" supported by Shanghai Education Development Foundation and Shanghai Municipal Education Commission (14CG30).

Notes and references

1 E. J. W. Crossland, N. Noel, V. Sivaram, T. Leijtens, J. A. Alexander-Webber and H. J. Snaith, *Nature*, 2013, **495**, 215-219.
2 X. Zheng, Q. Kuang, K. Yan, Y. Qiu, J. Qiu and S. Yang, *ACS Appl. Mater. Interfaces*, 2013, **5**, 11249-11257.
3 W. Jiao, Y. Xie, R. Chen, C. Zhen, G. Liu, X. Ma and H.-M. Cheng, *Chem. Commun.*, 2013, **49**, 11770-11772.
4 J. Pan, G. Liu, G. Q. Lu and H.-M. Cheng, *Angew. Chem. Int. Ed.*, 2011, **50**, 1-6.
5 B. Qiu, M. Xing and J. Zhang, *J. Am. Chem. Soc.*, 2014, **136**, 5852-5855.
6 H. Zhang, X. Lv, Y. Li, Y. Wang and J. Li, *ACS Nano*, 2009, **4**, 380-386.
7 Q. Xiang, J. Yu and M. Jaroniec, *J. Am. Chem. Soc.*, 2012, **134**, 6575-6578.
8 W. Li, F. Wang, S. Feng, J. Wang, Z. Sun, B. Li, Y. Li, J. Yang, A. A. Elzatahry, Y. Xia and D. Zhao, *J. Am. Chem. Soc.*, 2013, **135** 18300-18303.
9 K. K. Manga, J. Wang, M. Lin, J. Zhang, M. Nesladek, V. Nalla, W. Ji and K. P. Loh, *Adv. Mater.*, 2012, **24**, 1697-1702.
10 R. Mo, Z. Lei, K. Sun and D. Rooney, *Adv. Mater.*, 2014, **26**, 2084-2088.
11 J. S. Lee, K. H. You and C. B. Park, *Adv. Mater.*, 2012, **24**, 1084-1088.
12 S. Yang, X. Feng and K. Müllen, *Adv. Mater.*, 2011, **23**, 3575-3579.
13 H.-i. Kim, G.-h. Moon, D. Monllor-Satoca, Y. Park and W. Choi *J. Phys. Chem. C*, 2012, **116**, 1535-1543.
14 H. D. Jang, S. K. Kim, H. Chang, K.-M. Roh, J.-W. Choi and J. Huang, *Biosens. Bioelectron.*, 2012, **38**, 184-188.
15 J. Zhang, Z. Zhu, Y. Tang and X. Feng, *J. Mater. Chem. A*, 2013, **1**, 3752-3756.
16 G. Lui, J.-Y. Liao, A. Duan, Z. Zhang, M. Fowler and A. Yu, *J. Mater. Chem. A*, 2013, **1**, 12255-12262.
17 Y. T. Liang, B. K. Vijayan, K. A. Gray and M. C. Hersam, *Nano Lett.*, 2011, **11**, 2865-2870.
18 J. T.-W. Wang, J. M. Ball, E. M. Barea, A. Abate, J. A. Alexander-Webber, J. Huang, M. Saliba, I. Mora-Sero, J. Bisquert, H. J. Snaith and R. J. Nicholas, *Nano Lett.*, 2013, **14** 724-730.
19 M. Y. Xing, B. X. Yang, H. Yu, B. Z. Tian, S. Bagwasi, J. L. Zhang and X. Q. Gong, *J. Phys. Chem. Lett.*, 2013, **4**, 3910-3917.
20 T.-T. Wu, Y.-P. Xie, L.-C. Yin, G. Liu and H.-M. Cheng, *J. Phys. Chem. C*, 2015, **119**, 84-89.
21 D. Zhang, M. Yang and S. Dong, *J. Phys. Chem. C*, 2015, **119**, 1451-1456.
22 X. Yu, X. Han, Z. Zhao, J. Zhang, W. Guo, C. Pan, A. Li, H. Liu and Z. Lin Wang, *Nano Energy*, 2015, **11**, 19-27.
23 Z. Lai, F. Peng, H. Wang, H. Yu, S. Zhang and H. Zhao, *J. Mater. Chem. A*, 2013, **1**, 4182-4185.
24 M. Ramamoorthy, D. Vanderbilt and R. D. King-Smith, *Phys. Rev. B*, 1994, **49**, 16721-16727.
25 C. B. Mendive, T. Bredow, A. Feldhoff, M. Blesa and D. Bahnemann, *Phys. Chem. Chem. Phys.*, 2008, **10**, 1960-1974
26 M. Xing, F. Shen, B. Qiu and J. Zhang, *Sci. Rep.*, 2014, **4**, 6341
27 B. Qiu, Y. Zhou, Y. Ma, X. Yang, W. Sheng, M. Xing and J. Zhang, *Sci. Rep.*, 2015, **5**, 8591.
28 X. Wu, S. Yin, Q. Dong, B. Liu, Y. Wang, T. Sekino, S. W. Lee and T. Sato, *Sci. Rep.*, 2013, **3**, 2918.
29 J. Yu, G. Dai, Q. Xiang and M. Jaroniec, *J. Mater. Chem.*, 2011, **21**, 1049-1057.
30 Y. Zhang, P. Xiao, X. Zhou, D. Liu, B. B. Garcia and G. Cao, *J. Mater. Chem.*, 2009, **19**, 948-953.
31 S. Sakthivel and H. Kisch, *Angew. Chem. Int. Ed.*, 2003, **42**, 4908-4911.
32 M. Xing, J. Zhang, B. Qiu, B. Tian, M. Anpo and M. Che, *Small*, 2015, **11**, 1920–1929.
33 M. Xing, J. Zhang and F. Chen, *J. Phys. Chem. C*, 2009, **113**, 12848-12853.
34 Q. Xiang, J. Yu and M. Jaroniec, *Nanoscale*, 2011, **3**, 3670-3678.
35 Q. Xiang, J. Yu and M. Jaroniec, *Chem. Soc. Rev.*, 2012, **41**, 782-796.